American Mineralogist, Volume 92, pages 1007–1017, 2007

Dehydration of Ca-montmorillonite at the crystal scale. Part 2. Mechanisms and kinetics

Eric Ferrage,* Caroline A. Kirk, Gordon Cressey, and Javier Cuadros

The Natural History Museum, Department of Mineralogy, Cromwell Road, London SW7 5BD, U.K.

Abstract

A kinetic study of Ca-montmorillonite dehydration was performed based on information derived from X-ray diffraction (Ferrage et al. 2007, this issue) and, thus, focusing on interlayer water only. The dehydration was quantified following the two processes that were observed in the X-ray pattern modeling: the transitions between the different hydration states and small thickness decrease observed in the bi- and mono-hydrated layers. The thickness decrease of bihydrated layers with dehydration (activation energy E_a = 16 kJ/mol) was found to be controlled by a mechanism of two-dimensional diffusion of water molecules through the interlayer space, whereas for mono-hydrated layers the variation of thickness (E_a = 18 kJ/mol) occurred as a mechanism of slight local layer collapse and collapse propagation, attributed to a rearrangement of the configuration of the interlayer cation hydration shell. For the transition between the bi- and mono-hydrated state (E_a = 84 kJ/mol), the mechanism of reaction was found to evolve gradually with increasing temperature from local layer collapse and collapse propagation to a two-dimensional diffusion mechanism, as the forced diffusion of water molecules produced by the layer collapse transfers the control of the process to diffusion mechanism. This phenomenon causes the coexistence of two hydration states in a given interlayer. Finally, the transition between mono-hydrated and dehydrated layers (E_a = 132 kJ/mol) indicated the concomitance of water diffusion and local layer collapse and propagation mechanisms, although the structures were found to be homogeneous during this transition.

The determination of both mechanisms and the activation energy for these processes were used to establish a model of smectite dehydration at the crystal scale. This model can be used to calculate crystal shrinkage and interlayer water content upon dehydration, and to predict the evolution of the system.

Keywords: Crystal structure, smectite-water, diffusion, water in smectite interlayer, kinetics, smectite dehydration, mixed-layering, montmorillonite

Introduction

Smectite is important in controlling soil properties because of its high sorption, variable hydration states, and expansion behavior that can effectively re-seal cracks in the bulk material. For the same reasons, this mineral is a particularly useful component in the construction of waste barriers. Because smectite responds quickly to surrounding fluid conditions, the understanding of smectite hydration/dehydration is important in assessing the short- and long-term behavior of soils or engineered barriers where this mineral is present. Such understanding requires an accurate knowledge of all the dehydration processes occurring at the different scales (molecular, crystal, and centimeter-to-meter scale) and for the several ways in which water is linked to this mineral (water in the interlayer, on the external surface, in the micro- and macro-pores). Most of the studies dealing with the mechanism and kinetics of smectite dehydration were performed using thermal analysis, both isothermal (Guindy et al. 1985; Bray and Redfern 1999) and non-isothermal experiments (Poinsignon et al. 1982; Girgis et al. 1987; Laureiro et al. 1996; Zabat and Van Damme 2000). In these works the dehydration process was considered as occurring in a single event (Guindy et al. 1985; Girgis et al. 1987; Laureiro et al. 1996) or a two-step dehydration process (Poinsignon et al. 1982; Bray and Redfern 1999; Zabat and Van Damme 2000). Thermal analysis experiments cannot differentiate the water bound in different ways to smectite (i.e., water in the interlayer, on the external surface, and in micro- and macro-pores), as the information it provides about the activation energy represents an average of the removal processes of all the differently bonded water occurring in the sample. In contrast, the present study focuses on the dehydration process occurring at the crystal scale for water located exclusively in the interlayer of a Ca-saturated montmorillonite. At this scale of observation the smectite structure exhibits different hydration states, dehydrated = 0W, mono-hydrated = 1W, or bihydrated = 2W, corresponding to the intercalation of 0, 1, or 2 planes of water molecules in the interlayer. However, most often layers with different hydration states coexist within the same crystals. Therefore, the use of X-ray diffraction (XRD) profile modeling demonstrated in the companion paper (Ferrage et al. 2007) is necessary to assess and quantify the amount of water adsorbed in the smectite interlayer at any stage of the dehydration process. XRD patterns were thus recorded in the 30–170 °C temperature range in isothermal experiments and simulated using the algorithms developed initially

* E-mail: e.ferrage@nhm.ac.uk

by Sakharov and Drits (1973) and Drits and Sakharov (1976) and using the methodology recently developed by Ferrage (2004) and Ferrage et al. (2005). This method allows characterization of the structural modifications that occur during smectite dehydration, as layers transform between different hydration states and also allows measurement of the subtle decrease in thickness of hydrated layers that take place in response to the removal of a few water molecules (Ferrage et al. 2005, 2007a, 2007b). In this second part of the study we aim to use this substantial amount of information resulting from XRD profile modeling of dehydrating smectite to understand better the mechanisms and kinetics of the whole process. This approach will also be used to calculate the amount of crystal volume shrinkage upon dehydration and the amount of interlayer water remaining in the system.

Material and methods

The experimental procedure and subsequent XRD profile modeling is detailed in the first part of this study and can be resumed as follows: Samples of the <1 μm size fraction of Ca-saturated SWy-2 (a low-charge montmorillonite) were allowed to dry under room conditions (~25 °C and 60–65% RH) as oriented mounts and XRD snapshots recorded every 30 s under isothermal conditions (after equilibrium temperature was reached) from 30 to 170 °C, in steps of 5 °C. An additional isotherm was also recorded at 37 °C to optimize the data for one particular dehydration transition. Modification of the relative humidity with temperature close to the sample was not controlled. XRD profile modeling of the 00*l* reflections was applied for patterns collected in the 30–125 °C range (30 patterns per isotherm). XRD patterns collected for temperatures higher than 125 °C were not used because the sample started to dehydrate before reaching the desired temperature. The values for layer thickness of mono-hydrated (LT 1W) and bihydrated layers (LT 2W) were considered to be variable parameters in the calculations whereas that of dehydrated layers was considered to be constant at 9.7 Å. The uncertainty in relative abundance of layers was estimated to be ±2% when the abundance of the given layer is 100 or 0%, and ±5% when the layer represents 50% of the total layer contribution, with a linear dependence for intermediate values. The layer thickness uncertainty was estimated to be ±0.02 and ±0.05 Å when the given layer proportion is 100 and ~0% of the total layer contribution, respectively, with a linear dependence for intermediate values. The error propagation was considered for parameters calculated with these data.

Results

Empirical reaction rate of a solid-state reaction

In the part I of the present paper, the XRD profile modeling method allowed us to determine the proportion of 2W, 1W, and 0W layers, the layer thickness of 2W and 1W layers, and their water content in time-temperature space. With these data, we applied a data treatment similar to the isothermal gravimetric study of Bray and Redfern (1999) to build up a kinetic model and to better understand the mechanisms of smectite dehydration. For this kinetic analysis, the evolution of the relative proportions of 2W layers (%2W) and 0W layers (%0W) are chosen to define the 2W-1W and 1W-0W transitions, respectively. The evolution of the layer thickness of 1W (LT 1W) and 2W (LT 2W) layers are also considered.

For a solid-state reaction we can represent the reaction rate as a product of a function of the fraction transformed (α) and a rate constant (k):

$$d\alpha/dt = kf(\alpha). \quad (1)$$

The integrated form of Equation 1 (from time = 0 to time = t) can be expressed as:

$$g(\alpha) = kt \quad (2)$$

where the function $g(\alpha)$ depends on the mechanism of reaction (Sharp et al. 1966). One of the ways to perform the kinetic analysis is to fit the data to different rate equations $g(\alpha)$ and discriminate between the different mechanisms by the goodness of the fit (Hancock and Sharp 1972; Girgis et al. 1987; Girgis and Felix 1987; Laureiro et al. 1996; Gualtieri and Ferrari 2006, among others) Another way is to directly transform Equation 1 into an empirical equation in which the rate constant (k) and a parameter (m) that indicates the controlling reaction mechanism can be determined simultaneously (Avrami 1939; Hancock and Sharp 1972; Wilkinson et al. 1994; Belloto et al. 1995; Gualtieri et al. 1995; Miletich et al. 1997; Bray and Redfern 1999, 2000; Mazzucato et al. 1999; Fogg et al. 2000):

$$d\alpha/dt = k^m t^{m-1}(1 - \alpha). \quad (3)$$

The integration of Equation 3 leads to the expression of the fraction transformed α as:

$$\alpha = 1 - \exp[-(k t)^m]. \quad (4)$$

The value of the m parameter can thus be compared to the expected values for different types of solid-state reaction mechanisms defined by Sharp et al. (1966). Three general groups of reactions are usually defined. The first group includes the zero and first order as well as phase boundary reactions ($1.0 \leq m \leq 1.2$), whereas the second group includes diffusion-controlled reactions in one, two or three dimensions ($0.5 \leq m \leq 0.6$). Finally, the third group includes random nucleation reactions described by the Avrami equations (Avrami 1939): Equation 1 (m = 2.0) and Equation 2 (m = 3.0). Considering the layer structure of Ca-montmorillonite and the fact that the dehydration causes the collapse of the layers, the first order nucleation-growth reaction (F1) and the two-dimensional diffusion (D2) can be expected to control the process (Bray and Redfern 1999). The first order nucleation-growth reaction is considered an adequate mechanism because we can envisage that layer collapse starts at a certain point of the layer (nucleation) and then propagates laterally in the two dimensions (growth). The D2 process is obviously an appropriate mechanism as water needs to diffuse out of the interlayer space toward the edges of the crystal.

Determination of rate constants (k) and controlling reaction mechanism (m)

Equation 4 can be rewritten in its linearised form as:

$$\ln[-\ln(1 - \alpha)] = m \ln(t) + m \ln k. \quad (5)$$

A plot of $\ln[-\ln(1 - \alpha)]$ vs. $\ln(t)$ (t in seconds) is thus linear with a slope m and with a rate constant k corresponding to the intercept. To determine m and k for relevant temperatures, the data have first to be expressed as a function of α. This value ranges from 0, hydration state before the reaction starts, to 1, final hydration state at the corresponding temperature. This implies that it is necessary to characterize accurately the final, stable hydration state after the reaction. The hydration state will be

represented in the equations as some of the variables calculated in the XRD modeling process. Figure 5 in Ferrage et al. (2007) shows the evolution of the relative proportion of 2W, 1W, and 0W for the several isotherms. When using the change of these relative proportions with time for the kinetic analysis, not all the isotherms are equally useful. Some of them show a very quick reaction at the beginning of the experiment and then no or very small change. These isotherms are not useful because the greatest part of the reaction is recorded in the span of very few data points, which increases the uncertainty of the analysis. More interesting for our study are those isotherms in which the reaction is recorded in a large number of data points and the reaction progress can be constrained better. In addition, the evolution of the given parameter between the start and the end of reaction has to be significant to have sufficient sensitivity in the normalized α value. For instance the evolution of 2W layer abundance at the 30 °C isotherm is very limited (<3%, Fig. 5 in Ferrage et al. 2007) and the normalization of such set of data would lead to a very large uncertainty in the corresponding α values. These examples show that care has to be taken in the choice of the isotherms to which the kinetic analysis can be applied. For the relative contribution of 2W layers, the chosen experiments correspond to the temperatures between 35 and 50 °C. For the relative abundance of 0W layers, the isotherms chosen range from 90 to 110 °C. The temperatures above 110 °C were not considered because of the sudden variation of the data at the start of the experiments due to the fact that the sample starts to react before reaching the desired temperature. In the case of the analysis of the change of the layer thickness of 2W and 1W layers, the limiting factor for the use of a specific isotherm is the abundance of the given layer (Fig. 5 in Ferrage et al. 2007). This is so because the uncertainty of the layer thickness increases as the abundance of the layer decreases. Hence the isotherms considered are those between 30 and 40 °C, and between 45 and 95 °C for the thickness of 2W and 1W layers, respectively.

The values at equilibrium ($t = \infty$) of %2W, %0W, LT 2W, and LT 1W were determined, for each isotherm, by a least-square fitting of the data at times higher than 500 s, using the following formula (Miletich et al. 1997; Bray et al. 1998):

$$\delta^i_{t=\infty} = \delta^i_{(t_0)} + (\delta^i_{t_0} - \delta^i_{t=\infty}) \cdot \exp\{-[a(t - t_0)]^b\} \quad (6)$$

where i is the parameter considered (%2W, %0W, LT 2W or LT 1W), t_0 is 500 s, $\delta^i_{t_0}$ is the value of parameter i at 500 s, a and b are two parameters refined during the least-square procedure.

An example of the determination of the rate constant and m parameter is shown in Figure 1. The relative abundance of 2W layers at 35, 40, and 50 °C resulting from XRD profile modeling is shown in Figure 1a and the fraction transformed (α) in Figure 1b. The uncertainty of α shown in Figure 1b was determined by applying the linearization treatment on the maximum and minimum values derived from the uncertainty of the considered parameter shown in Figure 1a. The values of m and k are calculated from Equation 5 using the chosen isotherms, and are reported in Table 1. The value of m ranges between those of a first-order reaction (F1, m = 1) and a two-dimensional diffusion process (D2, m = 0.57), except for the evolution of %0W layers at temperature ≥ 100 °C. In addition, the m values tend to decrease with increasing temperature with the exception of those for LT1W, which are almost constant at ~1. Concerning reaction constants (k), the obtained values tend to increase with temperature and will be used below for determining activation energies.

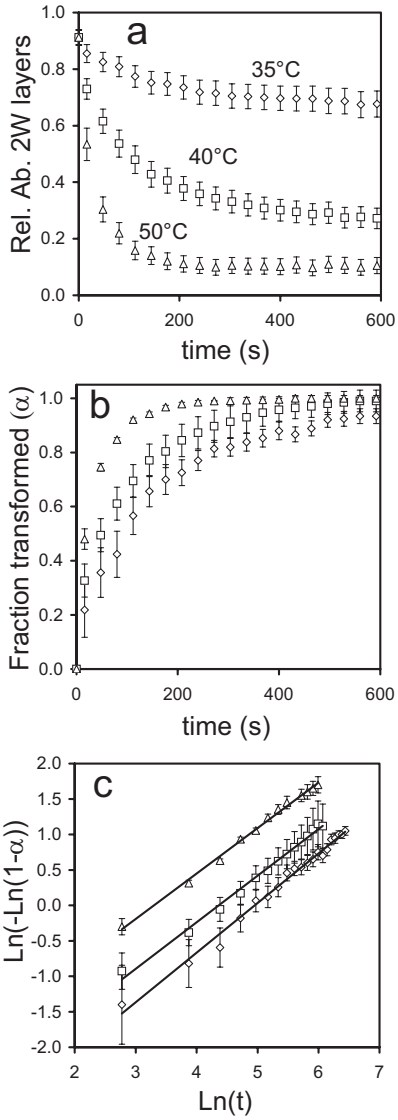

FIGURE 1. Example of plots for the determination of rate constants of smectite dehydration at three temperatures. (**a**) Evolution of the relative abundance of bihydrated layers determined from XRD profile modeling. (**b**)The same data after normalization with respect to the total extent of reaction in each isotherm. (**c**) Ln-ln plot of the same data to determine the rate constants and the exponent (m) of the Avrami equation, which indicates the reaction mechanism.

The evolution of the obtained values between the different parameters or as a function of temperature is related to specific water removal during dehydration and will be discussed below.

Determination of activation energy, E_a

The activation energies driving the different processes can be obtained using the Arrhenius equation:

Table 1. Values of the rate constant (*k*) and the parameter (m), which specifies the reaction mechanism, for the four variables analyzed (relative abundance of 2W and 0W layers and layer thickness of 2W and 1W layers)

T (°C)	%2W			*T* (°C)	LT 2W		
	k	m	r^2		*k*	m	r^2
35	$6.45(102)\cdot10^{-3}$	0.846(77)	0.870	30	$7.89(78)\cdot10^{-3}$	0.685(51)	0.906
37	$9.26(12)\cdot10^{-3}$	0.748(22)	0.985	35	$8.68(13)\cdot10^{-3}$	0.566(16)	0.980
40	$12.35(11)\cdot10^{-3}$	0.663(17)	0.992	37	$9.07(19)\cdot10^{-3}$	0.573(19)	0.972
45	$20.79(55)\cdot10^{-3}$	0.580(24)	0.974	40	$9.63(23)\cdot10^{-3}$	0.567(21)	0.985
50	$33.54(66)\cdot10^{-3}$	0.662(28)	0.982	–	–	–	
	–	–	–			LT 1W	
		%0W			*k*	m	r^2
	k	m	r^2	45	$1.53(3)\cdot10^{-3}$	0.969(32)	0.978
90	$1.55(8)\cdot10^{-3}$	0.733(36)	0.943	50	$1.69(6)\cdot10^{-3}$	0.960(40)	0.961
95	$3.09(6)\cdot10^{-3}$	0.778(24)	0.977	55	$1.85(7)\cdot10^{-3}$	0.938(42)	0.957
100	$4.93(13)\cdot10^{-3}$	0.452(17)	0.965	60	$2.22(9)\cdot10^{-3}$	1.020(46)	0.959
105	$9.92(12)\cdot10^{-3}$	0.344(9)	0.984	65	$2.36(17)\cdot10^{-3}$	1.054(63)	0.930
110	$15.80(18)\cdot10^{-3}$	0.310(8)	0.985	70	$2.53(17)\cdot10^{-3}$	0.922(53)	0.929
	–	–	–	75	$2.62(12)\cdot10^{-3}$	0.990(51)	0.966
	–	–	–	80	$3.02(3)\cdot10^{-3}$	1.001(24)	0.985
	–	–	–	85	$3.15(4)\cdot10^{-3}$	0.939(25)	0.983
	–	–	–	90	$3.65(4)\cdot10^{-3}$	1.074(26)	0.986
	–	–	–	95	$3.81(13)\cdot10^{-3}$	1.031(47)	0.975

$$k = A\exp(-E_a/RT) \quad (7)$$

or in its linearized form:

$$\ln k = \ln A - E_a/RT \quad (8)$$

where A is the frequency or pre-exponential factor (in s^{-1}) and E_a the activation energy (in J/mol), R the gas constant [8.31 J/(K·mol)], and T the temperature in Kelvin. By plotting ln$k$ vs. 1/T, E_a, and ln$A$ are calculated from the slope and the intercept, respectively (Fig. 2). The activation energy and pre-exponential factor of the different processes are reported in Table 2. For the variation of layer thickness, the activation energy values are found to be similar for 2W and 1W layers (Table 2). However, the activation energy of the 1W-0W transition is higher than that of the 2W-1W transition (Table 2).

Discussion

Smectite dehydration at the crystal scale is a complex process. XRD profile modeling has allowed the resolution of this process in its elementary stages. For Ca-montmorillonite, the transition from bihydrated to mono-hydrated state takes place at 30–50 °C, thereafter a mono-hydrated state dominates up to 85 °C (Fig. 5 in Ferrage et al. 2007). The transition from mono-hydrated to dehydrated state occurs above 85 °C. During the whole of this process the thickness of bi- and mono-hydrated layers evolves subtly as a result of the removal of some interlayer water molecules (Figs. 2 and 6 in Ferrage et al. 2007). This two-step mechanism parallels that described by Poinsignon et al. (1982), Bray and Redfern (1999) and Zabat and Van Damme (2000) based on the thermal analysis of Ca-smectite.

Mechanism of dehydration—m parameter

Although the Avrami method used here is empirical and may not allow the information on nucleation + crystal growth and rate limiting step to be determined univocally (Hulbert 1969; Gualtieri and Ferrari 2006), the m values determined in the present study can be used to describe the dehydration mechanism(s) occurring.

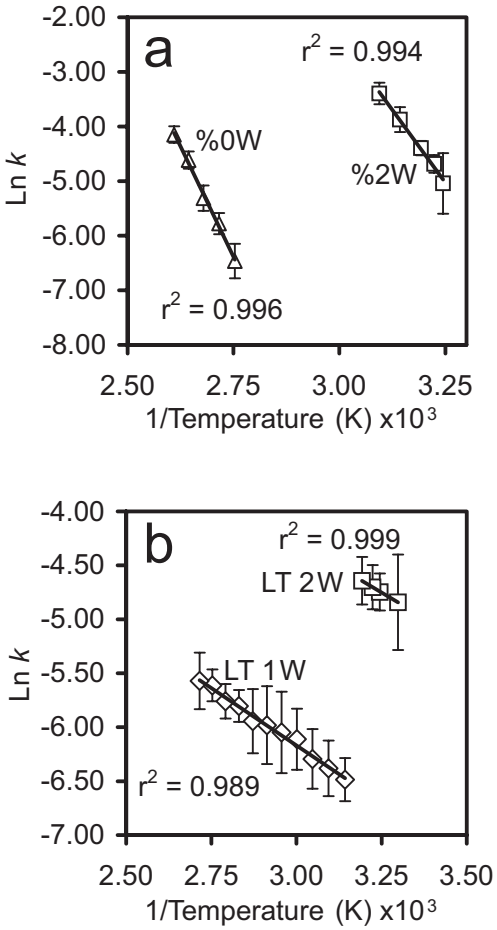

Figure 2. Arrhenius plot for the determination of the activation energy of the different processes occurring during dehydration. (**a**) 2W-1W and 1W-0W layer transitions. (**b**) Decrease of the layer thickness of bihydrated and mono-hydrated layers.

Hydration state transitions

The mechanism of the 2W-1W transition can be characterized by observing the disappearance of 2W layers with

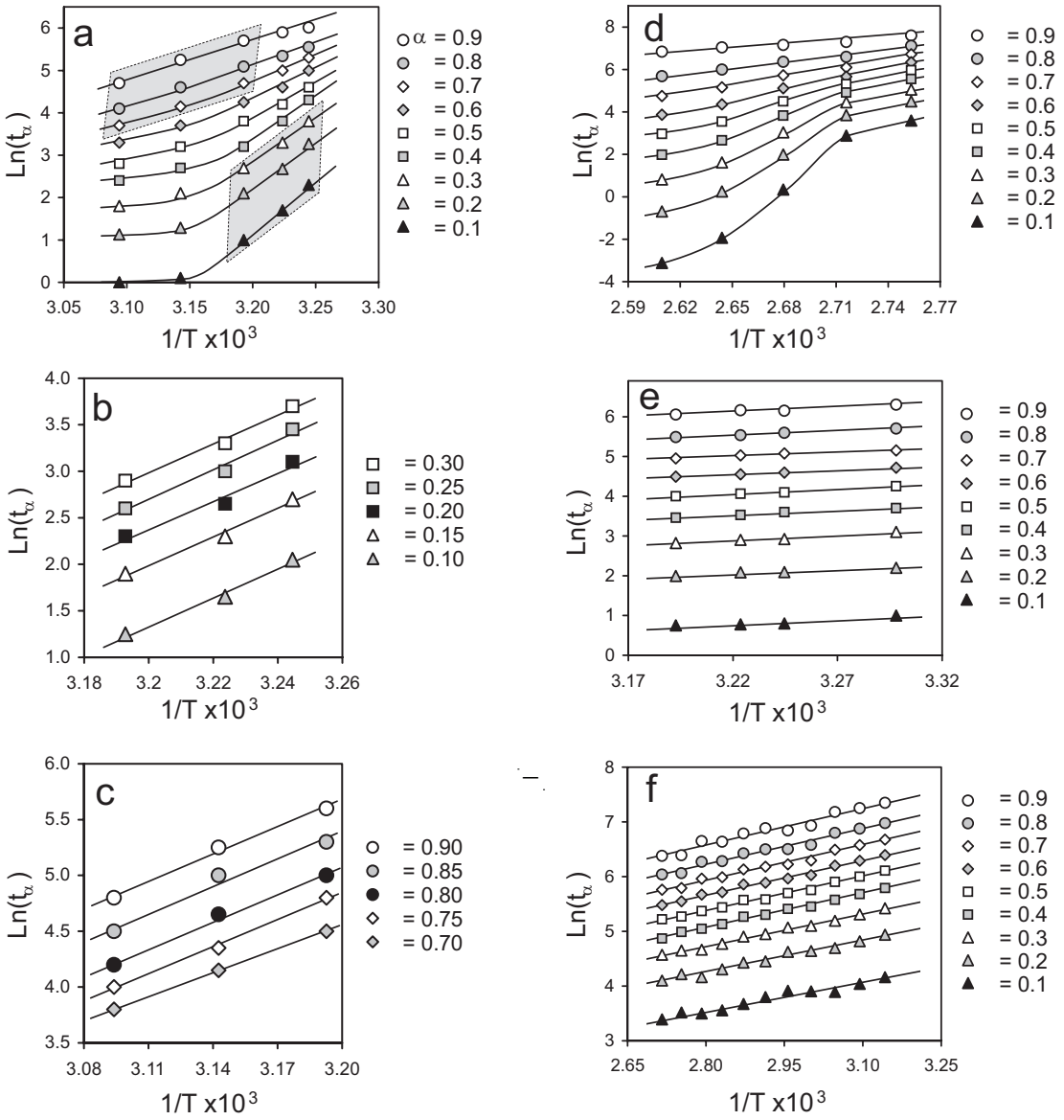

FIGURE 3. Isoconversional plots. (**a**) The 2W-1W layer transition for which the light gray regions are enlarged in (**b**) and (**c**) with additional α values. (**d**) The 1W-0W layer transition. (**e**) Decrease of the 2W layer thickness. (**f**) Decrease of 1W layer thickness. Temperature (*T*) is given in Kelvin.

increasing temperature. For this transition, the mean m value is ~0.70 (Table 2). Such value has no physical meaning because it does not correspond to any known solid-state reaction. This value is rather an intermediate one between that expected for a first-order nucleation-growth (m = 1) and a diffusion controlled process (m = 0.57). The observed gradual decrease of m with increasing temperature from 0.85 to 0.58 (Table 1) can thus be interpreted as a nucleation process of 1W layers that is slowed down by diffusion of water along the interlayer. If two mechanisms are concomitant in every single interlayer, the m value is mostly governed by the slower one. Therefore, with increasing temperature, the amount of water released in each interlayer by the nucleation of 1W layers increases and the speed of diffusion of these H_2O molecules toward the edges of the crystal has thus a greater control on the dehydration mechanism. The isoconversional method provides additional information to assess the actual presence of one or several concomitant mechanisms (Friedman 1964; Redfern 1987; Baitalow et al. 1999; Bray and

TABLE 2. Values of the m parameter, pre-exponential factor (*A*) and activation energy (E_a) for the analyzed variables *i* (relative abundance 2W and 0W layers and layer thickness of 2W and 1W layers), derived from XRD profile modeling

i	m	*A* (s^{-1})	E_a (kJ/mol)
%2W	0.70(10)	$1.25(4)\cdot10^{12}$	84(2)
%0W	0.76(3)	$1.90(8)\cdot10^{16}$	132(5)
LT 2W	0.60(6)	4.81(62)	16.2(5)
LT 1W	0.99(5)	1.34(87)	17.9(5)

Note: For the relative abundance of 0W layers, the value of m parameter was calculated as the mean of those obtained for 90 and 95 °C isotherms.

Redfern 1999; Simon 2004; Gualtieri and Ferrari 2006, among others). The fraction transformed (α) and the time (t) are obviously related through a function. By combination of Equations 1 and 7 it is possible to write:

$$d\alpha/dt = A\exp(-E_a/RT)\, f(\alpha). \quad (9)$$

By integration of Equation 9, the time (t_α) at which the conversion α is reached can be expressed as:

$$\ln(t_\alpha) = -E_a/RT - \ln[A/g(\alpha)]. \quad (10)$$

The method uses a plot of $\ln(t_\alpha)$ against $(1/T)$. If the plot is linear, the activation energy, and thus the mechanism, does not change for the chosen range of temperature and fraction transformation. The advantage of this method is that it is model-independent, i.e., it does not depend on the function linking α and t (f or g in Eqs. 9 and 10). This plot is shown for the 2W-1W transition in Figure 3a. The data display two slopes for α values lower than 0.7 and one slope for higher α values. The existence of two slopes in a line shows that there are at least two mechanisms implicated. The first mechanism is best observed for $35 \le T \le 40$ °C and $0.1 \le \alpha \le 0.3$ in Figure 3b. The slopes in this part of the lines yield an activation energy of 128 ± 4 kJ/mol. The second mechanism (Fig. 3c) can be characterized using data for $0.7 \le \alpha \le 0.9$ and $40 \le T \le 50$ °C and produces an activation energy of ~66 ± 4 kJ/mol. The use of the isoconversional method therefore supports the existence of two concomitant mechanisms, described before as nucleation of 1W layers and water diffusion. They control the reaction kinetics sequentially for low α values, nucleation at the lower temperature and diffusion at the higher temperature (Fig. 1c, Table 1), whereas only diffusion controls the reaction at high α values. The activation energy found using the Avrami method of ~84 ± 2 kJ/mol (Table 2) for the 2W-1W transition is thus intermediate between those of the two individual processes involved in the reaction.

In the 1W-0W transition, the increase of 0W layers produces a range of m parameter values between 0.73 and 0.31 (Table 1). A value lower than that expected for a pure diffusion process (m ~0.5) does not reflect any specific rate law. The isotherms at 100–110°C present an apparent sudden increase of layers with %0W, which is due to the dehydration reaction starting before the desired temperature is reached (Fig. 5 in Ferrage et al. 2007). Using the isoconversional method again two slopes appear for low α values whereas a single line fits the data for higher α values (Fig. 3d). However, for α values lower than 0.5, the evolution of $\ln(t_\alpha)$ for temperatures higher than 95 °C is a curved line. This shape could be due to the fact that, at this experimental temperature range, the sample dehydrates partially before reaching the desired temperature. For this reason, this method cannot be applied to discriminate between one or two processes and to determine their activation energy. Additional work using linear heating would be necessary to investigate dehydration at this high temperature. However, even though it is not possible to assess the presence of two concomitant reactions with the isoconversional method, as for the 2W-1W transition, the m parameter value close to 0.75 obtained for data recorded at $90 \le T \le 95$ °C may indicate a similar two-step reaction.

Layer thickness evolution

The layer thickness of bihydrated layers shows a stable value of m between 35 and 40 °C (~0.57 – Table 1), corresponding to a two-dimensional diffusion reaction. Although for the isotherm recorded at 30 °C the m value close to 0.68 may correspond to a coupled nucleation-growth and diffusion process, the isoconversional method shows that data lie on a single line (Fig. 3e), supporting that a unique mechanism (i.e., the two-dimensional diffusion) governs the process. Finally, for mono-hydrated layers, a constant value of m was found between 0.92 and 1.05 through the entire range of temperature (45–95 °C; Table 1). The isoconversional method shown in Figure 3f supports the presence of such single mechanism, related to a first-order reaction. This mechanism is likely to be related to a modification of layer thickness as a result of the removal of interlayer water and reorganization of water coordination around the interlayer cation (see below).

Sequential evolution of the dehydration process

The determination of the two mechanisms controlling hydration state transitions and layer thickness evolution can be considered together with the description of the evolution of the smectite-water structure from Part 1 to draw a sequential path for the dehydration dynamics (Fig. 4). For low temperatures the structure consists almost completely of bihydrated layers (Figs. 4a and 4b). Figure 6a in Ferrage et al. (2007) showed that some H_2O molecules are coordinated to the interlayer cation but a large amount of them are filling the interstitial space. With a slight increase of the temperature, the layer thickness decreases as a result of the removal of some of these water molecules. It can be assumed that, in the 2W state, the large amount of water in the interlayer space and the multiple H-bonding that can link a water molecule with the clay surface or other H_2O molecules can complicate its pathway to exit the interlayer. This difficulty may explain the dominant diffusion-type reaction obtained for this process (Table 2). At some stage of the dehydration process, it is possible to assume that a few interlayer cations in the 2W layer have lost enough water and that the attractive force with the 2:1 clay surface may thus dominate, inducing a local collapse of the interlayer (Fig. 4c). This phenomenon is responsible for the transition of a few 2W layers into the mono-hydrated state whereas the other layers continue to dehydrate slightly in the 2W configuration. Note that this collapse occurs although non-coordinated water molecules are still present in the interlayer (Ferrage et al. 2007). The 2W-1W transition may thus start close to a cation and propagate to the adjacent cations in the interlayer as a collapse-propagation first-order reaction. The H_2O molecules that are being expelled are likely to diffuse through the interlayer space following a two-dimensional diffusion process, as determined for the variation in 2W layer thickness. However with an increasing amount of water forced to diffuse away by the collapse of the layer, water molecules would diffuse with more difficulty and cause a greater control of the diffusion mechanism (lower m with increasing temperature, Table 1, and change of slope with increasing α values and temperature in the isoconversional plot, Fig. 3a). In addition, the partial collapse (variable hydration state) within the same interlayers is likely to be responsible for the apparent increase of structural heterogeneity and the high

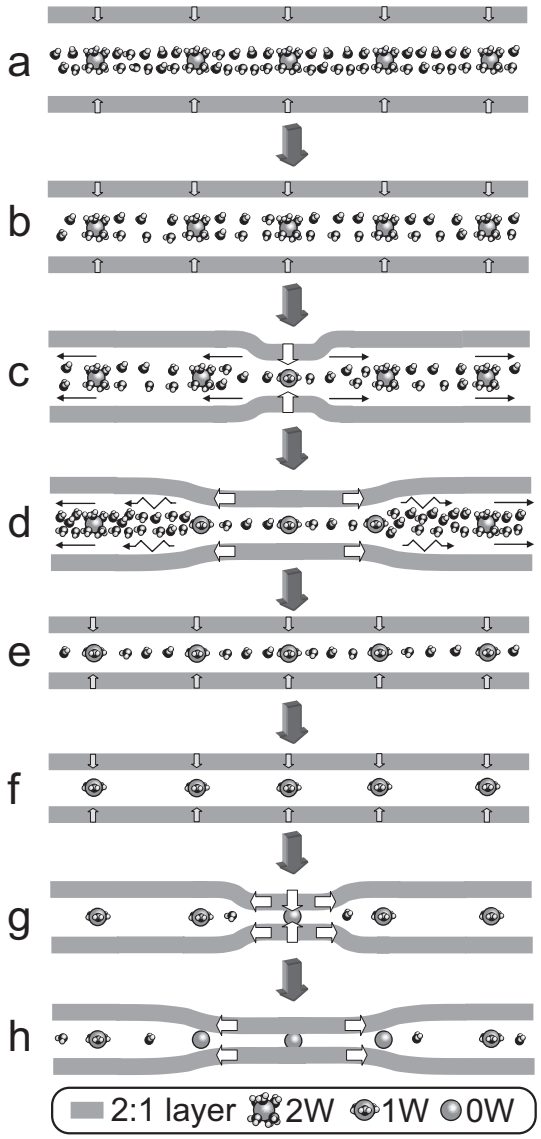

FIGURE 4. Sequential path of Ca-montmorillonite dehydration at the layer scale. Cations and water molecules are not shown to scale and their distribution within the interlayer is only schematic. Initially, most layers are bihydrated. As temperature increases a slight removal of water molecules following a diffusion process induces a decrease in layer thickness (**a**,**b**). At some stage of the dehydration a few cations in part of the interlayer region lose some of their water shell starting the transition to the mono-hydrated state (**c**, **d**). The transition initiates a collapse around this interlayer cation (**c**) and propagates to the adjacent cations. Water molecules are pushed laterally by this collapse but diffuse slowly and accumulate within the interlayer space, which produces a modification of the controlling mechanism from first-order to diffusion (**d**). The first mono-hydrated layers produced have water molecules directly bonded to the interlayer cation and additional water molecules within void spaces (**e**). As the dehydration process continues, these additional water molecules diffuse away and there is a rearrangement of the configuration of the hydration shell of the interlayer cation that causes a small decrease of the interlayer space (**f**). Finally the transition between the mono-hydrated and the dehydrated state occurs as a combined first-order and diffusion process (**g**, **h**), in a similar fashion to the 2W-1W transition.

values of the layer thickness fluctuation (σ_z parameter; Fig. 2j in Ferrage et al. 2007).

When the 2W-1W transition starts to take place, the first layers reaching the mono-hydrated state (Fig. 4e) contain some additional non-coordinated H_2O molecules, as determined from the number of water molecules per interlayer cation (Fig. 6a in Ferrage et al. 2007). Then a stable 1W state is observed between 45 and 85 °C although a decrease in layer thickness is observed together with a decrease in water content from ~8 to ~4 water molecules per cation. At this stage it may be assumed that most water molecules are linked to the interlayer cations (Fig. 4f). The kinetic analysis has revealed a pure first-order reaction for the small reduction of the layer thickness of 1W layers (Table 1). The removal of these few water molecules may thus occur as a nucleation-growth process by a successive removal of one H_2O molecule from the hydration shell of each interlayer cation. This local dehydration is likely to be accompanied by a coordination rearrangement of the water molecules around the interlayer cation as shown by Rausell-Colom et al. (1980) on Ca-saturated vermiculite sample. Finally, the 1W-0W transition (Figs. 4g and 4h) starts once the limit of ~4 water molecules per cation is reached (Fig. 6a in Ferrage et al. 2007). Although not as clear for the 2W-1W transition, this one may occur as a two-step process, with a first-order and then a diffusion reaction (Table 1). The first-order reaction is likely to represent the collapse of the layer around an interlayer cation and the propagation of this collapse toward the adjacent cations. Two possible reasons may account for the diffusion type process. First, it may be assumed that, below ~4 water molecules per cation, the interlayer cations may attract water molecules very effectively and the removal of water may thus be slowed down by successive jumps of a given water molecule from one interlayer cation to another in its path to the edges of the crystal. The second reason may arise directly from the collapse of the layer that limits the volume available for the diffusion of the water molecules. During this stage of dehydration, the lower amount of water present may diffuse more easily and thus be responsible for the apparent homogeneous 1W-0W transition within a given interlayer, in agreement with the low values obtained for layer thickness fluctuation (σ_z parameter—Fig. 2j in Ferrage et al. 2007). Thus, the transition depicted in Figures 3g and 4h (1W-0W transition) is faster than that in Figures 4c and 4d (2W-1W transition), so that very few interlayers show the coexistence of 1W and 0W states at any given moment.

Activation energy of the observed processes

The activation energy values of the transition reactions are 84 ± 2 and 132 ± 5 kJ/mol for the 2W-1W and the 1W-0W transition, respectively (Table 2). Because these transformations contribute in a major way to the release of water compared to the loss of the more loosely bound interlayer water that induces only a slight decrease of layer thickness, these activation energies can be compared with others determined for Ca-montmorillonites in the literature (Table 3). For this comparison, only studies that take into account dehydration in two steps were considered. For the first dehydration reaction, the activation energy determined in the present study is higher than those observed by Bray and Redfern (1999) and Poinsignon et al. (1982; ~35

and 37 kJ/mol, respectively) but similar or slightly lower to that obtained by Zabat and Van Damme (2000; 84 kJ/mol, Table 3). On the other hand the activation energy value determined for the 1W-0W transition is lower than that obtained by Poinsignon et al. (1982; 185 kJ/mol) but higher than those observed by Bray and Redfern (1999) and Zabat and Van Damme (2000; 47 and 91 kJ/mol, respectively, Table 3). In addition note that Bray and Redfern (1999) determined that dehydration in montmorillonite occurred controlled by two concomitant mechanisms, nucleation and growth followed by a diffusion-controlled reaction. This interpretation is similar to that in the present study for 2W-1W and 1W-0W transitions. The differences in activation energy values may be related to the type of technique used and the data treatment applied to derive those activation energies. Indeed these authors used techniques based on thermal analysis, which probe water adsorbed in the interlayer, on the external surfaces and in micro- and macro-pores, whereas XRD only detects water located in the interlayer. It is thus possible to assume that the influence of water loosely bonded on the external surface or between particles decreases the overall activation energy of dehydration taking place at low temperature. In addition, other parameters may influence the activation energy determined such as: the recording mode (isothermal vs. dynamic heating), the heating rate and the relative humidity conditions of the experiment. Therefore a precise comparison between all the data obtained is difficult although the values determined in this study are in range with those determined in the literature.

The activation energy values determined for the evolution of mono-hydrated and bihydrated layer thickness are similar (Table 2). This may indicate that the two reactions involve similar types of local hydrogen-bonding interactions. For 1W layers, these interactions affect water forming the hydration shell of the interlayer cation. As the activation energy is similar for the 2W layers, it may be considered that, in the latter layer type, only (first-shell) water directly linked to the interlayer cation controls the interlayer thickness.

Numerical model for smectite crystal dehydration and its applications

Empirical model for crystal dehydration

The evolution of the proportion of 2W, 1W, and 0W layers as a function of temperature indicates that the samples either reach an equilibrium state at the end of each experiment or are very close to it (Fig. 5 in Ferrage et al. 2007). To build up a kinetic model for the structural dehydration of smectite, it is necessary to determine the evolution of the equilibrium value for the layer thickness of 1W and 2W layers and the relative proportion of 2W and 0W layers. The evolution of the $\delta^i_{t=\infty}$ values determined above from a least square fitting of Equation 6 is plotted in Figure 5 as a function of temperature. To compute the observed evolution of the several parameters, the data are fitted, by a least square fitting procedure, to a sigmoid function based on the Boltzmann model:

$$\delta^i_{(T,t=\infty)} = \delta^i_{(T\max,t=\infty)} + [\delta^i_{(T\min,t=\infty)} - \delta^i_{(T\max,t=\infty)}] / \{1+\exp[(T - T_0)/\Delta T]\} \quad (11)$$

where $\delta^i_{(T,t=\infty)}$ is the value of the parameter i (%0W, %2W, LT 2W, LT 1W) at equilibrium ($t = \infty$) as a function of temperature (T, in Kelvin), $\delta^i_{(T\min,t=\infty)}$ and $\delta^i_{(T\max,t=\infty)}$ represent the expected values at the minimum and maximum temperature, T_0 is the center of the sigmoid curve and ΔT the width of the sigmoid curve (in Kelvin). The best-fit parameters are reported in Table 4.

By combining Equations 4, 7, and 11 the evolution of LT 2W, LT 1W, and %2W can be expressed as a function of time (in seconds) and temperature (in Kelvin) using the m, E_a, and A parameters in Table 2, the $\delta^i_{(T,t=\infty)}$ values from Equation 11 and parameters reported in Table 4:

$$\delta^i_{(T,t)} = \delta^i_{(T\min,t=\infty)} - [\delta^i_{(T\min,t=\infty)} - \delta^i_{(T,t=\infty)}] \times \{1 - \exp[-(A^i \cdot \exp(-E^i_a/RT) \times t)^m]\} \quad (12)$$

Note that for the kinetic parameters of the 2W-1W and 1W-0W transition reactions in Table 2, the values of m, A, and E_a represent average kinetic parameters involving two mechanisms. As a result, the values of m (calculated as a mean value from all temperatures for the 2W-1W transition and from the 90 and 95 °C isotherms for the 1W-0W transitions and, ranging between those expected for F1 and D2 processes, 1.0 and 0.5, respectively) do not have a physical meaning and are used here for simplicity.

For the determination of the relative abundance of 0W layers Equation 12 becomes:

$$\delta^{\%0W}_{(T,t)} = \delta^{\%0W}_{(T\min,t=\infty)} + [\delta^{\%0W}_{(T,t=\infty)} - \delta^{\%0W}_{(T\min,t=\infty)}] \times \{1 - \exp[-(A^{\%0W} \cdot \exp(-E^{\%0W}_a/RT) \times t)^m]\} \quad (13)$$

The relative abundance of 1W layers is therefore logically determined as:

$$\delta^{\%1W}_{(T,t)} = 1 - \delta^{\%2W}_{(T,t)} - \delta^{\%0W}_{(T,t)} \quad (14)$$

As we have considered a fixed thickness for the dehydrated layers of 9.7 Å, the average layer thickness (in angstroms) in the crystal can be expressed as:

$$\delta^{\text{Thick.}}_{(T,t)} = \delta^{\%2W}_{(T,t)} \times \delta^{LT\ 2W}_{(T,t)} + \delta^{\%1W}_{(T,t)} \times \delta^{LT\ 1W}_{(T,t)} + \delta^{\%0W}_{(T,t)} \times 9.7 . \quad (15)$$

Validity of parameters derived from the kinetic analysis is proven by the inversion of Equations 12, 13, and 14, for the evolution of the relative abundance of layers at 37 and 95 °C in

Table 3. Activation energy of Ca-montmorillonite dehydration from this and other studies

Sample	Technique	E_a (kJ/mol), First dehydration step	E_a (kJ/mol), Second dehydration step	Authors
Ca-montmorillonite (<2 µm)	Isothermal thermogravimetry	35.5(5)	47(6)	Bray and Redfern (1999)
Ca-montmorillonite (<2 µm)	Dynamic thermogravimetry	71	91	Zabat and Van Damme (2000)
Ca-montmorillonite (<2 µm)	Differential Thermal Analysis	37	185	Poinsignon et al. (1982)
Ca-montmorillonite (<1 µm)	Isothermal XRD	84(2)	127(5)	This study

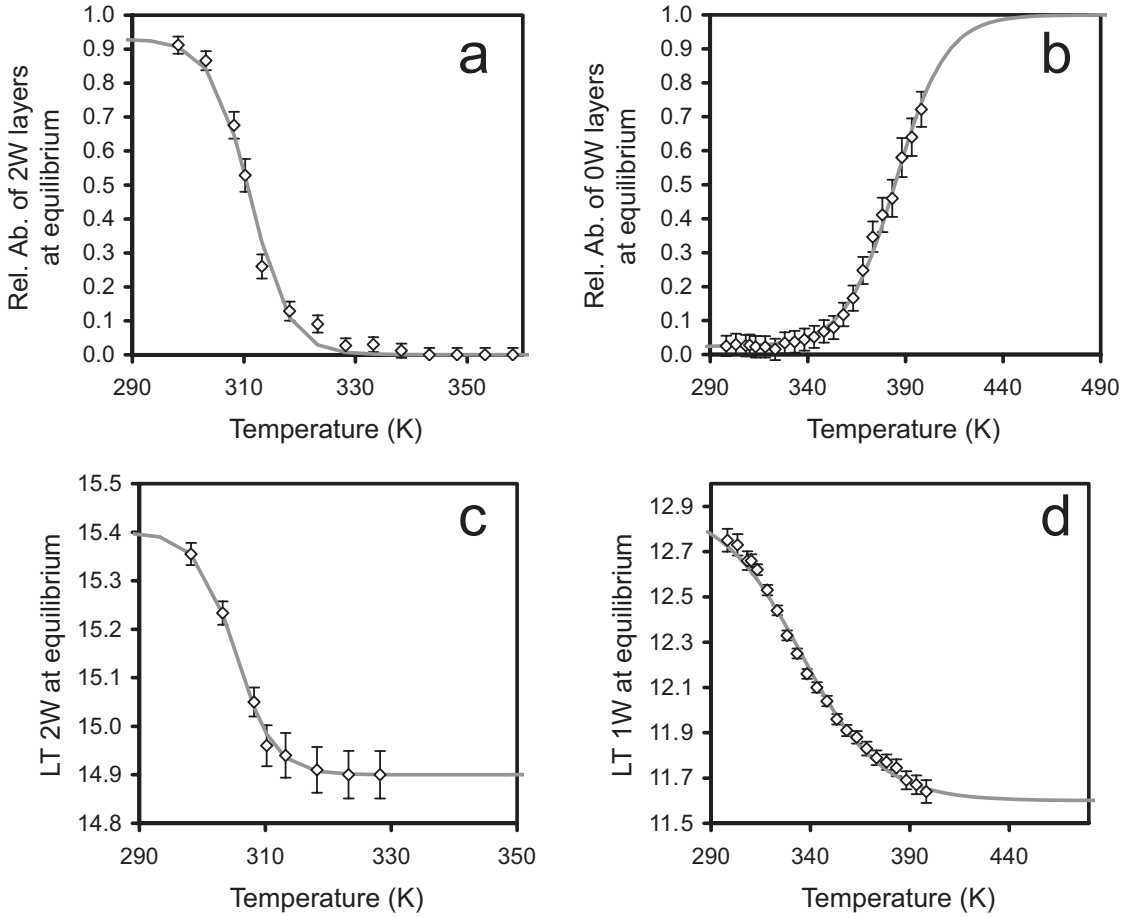

FIGURE 5. Calculated values of some parameters at $t = \infty$ from Equation 6, as a function of temperature. The lines are a best fit using Equation 11.

TABLE 4. Parameters used to calculate the equilibrated values at $t = \infty$ using Equation 11 for the fourth variables i (relative abundance 2W and 0W layers and layer thickness of 2W and 1W layers)

i	$\delta_{i(Tmin,t=\infty)}$	$\delta_{i(Tmax,t=\infty)}$	T_0	ΔT	r^2
% 2W	0.93	0.00	311.13(28)	3.51(24)	0.994
% 0W	0.024	1.00	385.15(43)	12.83(36)	0.996
LT 2W	15.40	14.90	305.30(11)	3.07(10)	0.997
LT 1W	12.90	11.60	335.23(38)	20.00(35)	0.995

Figure 6. The original values obtained from XRD modeling fit very well the calculated equations and these kinetic parameters can thus be used confidently for further prediction. However, because the system reaches the equilibrium very fast, the values obtained at the maximum experimental time are more applicable to natural conditions.

Implications of the defined model for natural conditions

The prediction of volume change and water release in soil and smectite-based waste barriers are the two most important parameters that need to be established. Indeed, the change in volume can induce a dramatic modification of the texture by the formation of cracks and lead to a much reduced efficiency of the waste barrier.

From Equation 15, the average layer thickness (in angstroms) at maximum time can be expressed as a function of temperature as:

$$\delta^{\text{Thick.}}_{(T,t=\infty)} = \delta^{\%2W}_{(T,t=\infty)} \times \delta^{LT\ 2W}_{(T,t=\infty)} + \delta^{\%1W}_{(T,t=\infty)} \times \delta^{LT\ 1W}_{(T,t=\infty)} + \delta^{\%0W}_{(T,t=\infty)} \times 9.7 . \quad (16)$$

In Figure 7a, the layer thickness calculated with Equation 16 is shown with the corresponding data from the expected values at $t = \infty$ derived from Equation 6. For temperature near 45 °C, this model indicates a total variation of the average crystal thickness of about 15%. Note that the combination of a temperate climate ($T < 35$ °C) and low humidity in the atmosphere could easily lead to these changes. For higher temperature conditions as in nuclear waste repositories the reduction of smectite layer thickness would be of about 25% and 35% at 100 and 150 °C, respectively. Obviously, this study is only concerned with the behavior of smectite crystals in an open atmosphere where water can evaporate and diffuse away. Additional investigation is necessary to assess the effect of a confined system and of the corresponding crystal shrinking on the micro- and macropore sizes and on the clay texture, to assess the possible development of cracks.

Although the water content is best quantified using water vapor adsorption-desorption experiments (Bérend et al. 1995, Cases et al. 1992, 1997; Michot et al. 2005; Rinnert et al. 2005), it was shown in part 1 of the present paper that an approximate

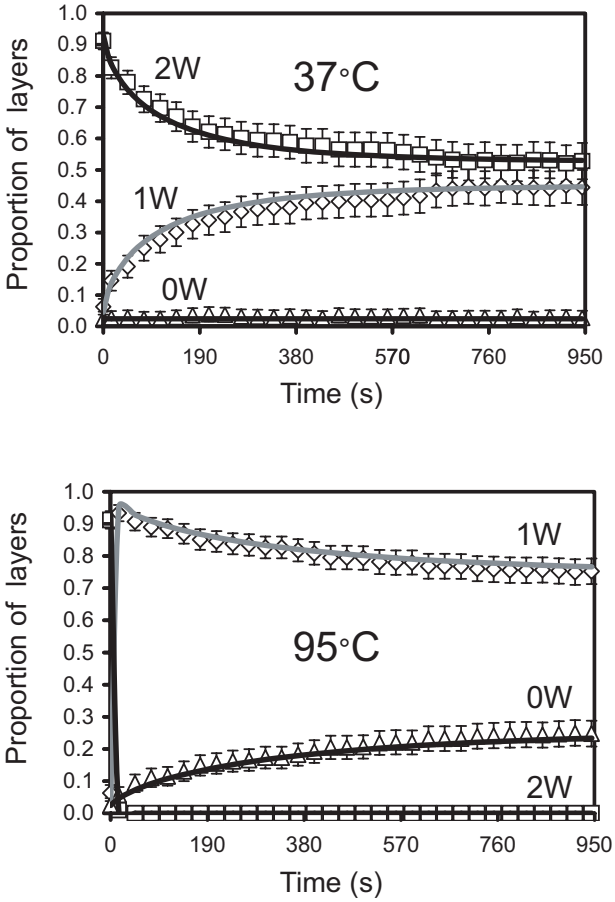

FIGURE 6. Calculated proportion of layers in the several hydration states vs. time, for two selected temperatures. The lines and the symbols correspond to the predicted values from Equations 12, 13, and 14 and to values obtained from XRD profile modeling, respectively.

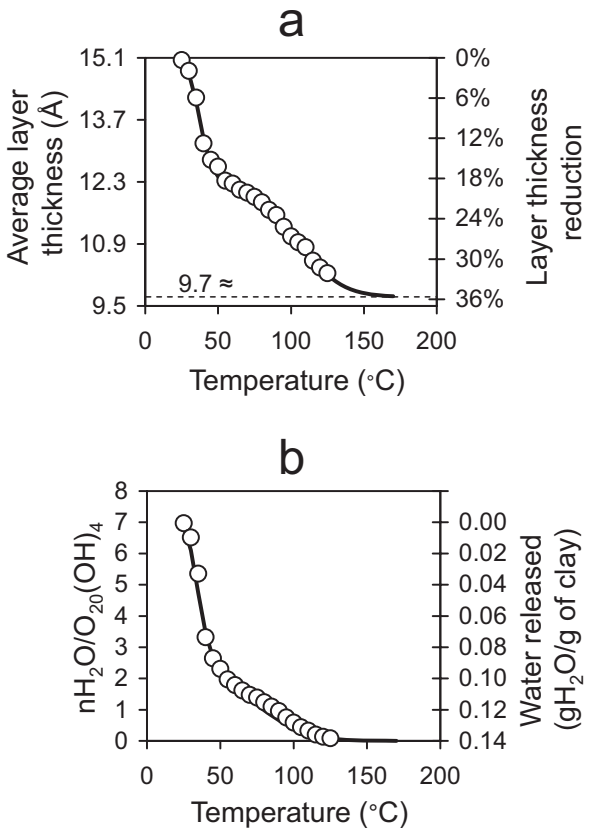

FIGURE 7. (**a**) Average layer thickness and (**b**) the corresponding water content released as a function of temperature. The lines are calculated with Equations 16 and 20, respectively and represent the predicted values from the proposed model. Open symbols represent extrapolated values at t = ∞ from the XRD profile modeling procedure using Equation 6.

linear correlation could be found between the layer thicknesses of 1W and 2W layers and the total layer water content (Fig. 6 in Ferrage et al. 2007). This correlation can be used to derive the interlayer water content as a function of temperature. According to this correlation, the contribution of water content from mono-hydrated layers can be expressed as:

$$\delta^{nH_2O\ (1W)}_{(T,\,t=\infty)} = \delta^{\%1W}_{(T,\,t=\infty)} \times \left[\delta^{LT\ 1W}_{(T,\,t=\infty)} \times 2.46 - 28.38\right]. \quad (17)$$

And the contribution from bihydrated layers is:

$$\delta^{nH_2O\ (2W)}_{(T,\,t=\infty)} = \delta^{\%2W}_{(T,\,t=\infty)} \times \left[\delta^{LT\ 2W}_{(T,\,t=\infty)} \times 4.46 - 61.14\right]. \quad (18)$$

Because the water content in 0W layer is null, the total amount of water in the system is:

$$\delta^{nH_2O\ Tot.}_{(T,\,t=\infty)} = \delta^{nH_2O\ (1W)}_{(T,\,t=\infty)} + \delta^{nH_2O\ (2W)}_{(T,\,t=\infty)}. \quad (19)$$

This is the amount of water per unit cell, which can be transformed into a more representative unit; for example, in grams of water released per gram of clay. Thus, from Equation 19:

$$\delta^{nH_2O\ \text{Tot.}}_{(T,\ t=\infty)} = \left[\delta^{nH_2O\ (1W)}_{(T=298.21\ \text{K},\,t=\infty)} - \delta^{nH_2O\ (1W)}_{(T,\,t=\infty)}\right] \times 18 / M_{1W} + \left[\delta^{nH_2O\ (2W)}_{(T=298.21\ \text{K},\,t=\infty)} - \delta^{nH_2O\ (2W)}_{(T,\,t=\infty)}\right] \times 18 / M_{2W} \quad (20)$$

where the total water amount released is then expressed as grams of water per gram of clay or liters of water per kilogram of clay as respect to the fully hydrated state (initial state). The equations

$$\delta^{nH_2O\ (1W)}_{(T=298.21\ \text{K},\,t=\infty)}$$

and

$$\delta^{nH_2O\ (2W)}_{(T=298.21\ \text{K},\,t=\infty)}$$

represent the initial water content for mono-hydrated and bihydrated layers, respectively, determined at 25 °C using Equations 17 and 18. M_{1W} and M_{2W} represent the molecular weight of mono-hydrated and bihydrated layers based on their water content at $t = 0$ (initial state).

Figure 7b shows the data points from the XRD modeling and the calculated lines using Equation 20. For temperatures less than 45 °C, the amount of water released, determined using this model, represents about 80 mL per kilogram of clay. For higher temperatures, up to 100 °C, 130 mL of water per kilogram of clay could be released. If this evaporated water could condense somewhere else within the clay matrix, it could lead to additional processes of pollutant transport or local dissolution.

Further development of the proposed model for application to natural systems

The empirical models of layer thickness and water released evolution can be used to predict the evolution of the system at the crystal scale in a natural context. As discussed by Ferrage et al. (2007), the global path of smectite dehydration seems to be similar whatever the cause of dehydration (increasing temperature at constant humidity or decreasing relative humidity at constant temperature) although the final hydration state differs depending on the specific physical conditions. As the hydration state depends mainly on the nature of the interlayer cation and relative humidity, their influence needs to be assessed. Studies of smectite dehydration in variable conditions and with different interlayer cations could be integrated to create a comprehensive model of the process at the crystal scale. Finally, supplementary studies would be necessary to assess the influence of the decrease of crystal swelling on macroscopic textural modification.

Acknowledgments

This study was funded by a Marie-Curie Intra-European fellowship granted to E.F. (contract: MEIF-CT-2004-515386).We are grateful to Marc Blanchard (Royal Institute, London, U.K.) for fruitful discussions about kinetics and diffusion processes in minerals. The manuscript was much improved by the constructive reviews of Alessandro Gualtieri and an anonymous reviewer. The editorial assistance of AE Warren Huff is acknowledged.

References cited

Avrami, M. (1939) Kinetics of phase change. I. General theory. Journal of Chemical Physics, 7, 1103–1112.

Baitalow, F., Schmidt, H.G., and Wolf, G. (1999) Formal kinetic analysis of processes in the solid state. Thermochimica Acta, 337, 111–120.

Belloto, M., Gualtieri, A.F., Artioli, G., and Clark, S.M. (1995) Kinetic study of the kaolinite-mullite reaction sequence. Part I: Kaolinite dehydroxylation. Physics and Chemistry of Minerals, 22, 207–214.

Bérend, I., Cases, J.M., François, M., Uriot, J.P., Michot, L.J., Masion, A., and Thomas, F. (1995) Mechanism of adsorption and desorption of water vapour by homoionic montmorillonites: 2. The Li^+, Na^+, K^+, Rb^+ and Cs^+ exchanged forms. Clays and Clay Minerals, 43, 324–336.

Bray, H.J. and Redfern, S.A.T. (1999) Kinetics of dehydration of Ca-montmorillonite. Physics and Chemistry of Minerals, 26, 591–600.

——— (2000) Influence of conterion species on the dehydroxylation of Ca^{2+}-, Mg^{2+}-, Na^+- and K^+-exchanged Wyoming montmorillonite. Mineralogical Magazine, 64, 337–346.

Bray, H.J., Redfern, S.A.T., and Clark, S.M. (1998) The kinetics of dehydration in Ca-montmorillonite: an in situ X-ray diffraction study. Mineralogical Magazine, 62, 647–656.

Cases, J.M., Bérend, I., Besson, G., François, M., Uriot, J.P., Thomas, F., and Poirier, J.P. (1992) Mechanism of adsorption-desorption of water vapor by homoionic montmorillonite. 1. The sodium exchanged form. Langmuir, 8, 2730–2739.

Cases, J.M., Bérend, I., François, M., Uriot, J.P., Michot, L.J., and Thomas, F. (1997) Mechanism of adsorption and desorption of water vapour by homoionic montmorillonite: 3. the Mg^{2+}, Ca^{2+}, Sr^{2+} and Ba^{2+} exchanged forms. Clays and Clay Minerals, 45, 8–22.

Drits, V.A. and Sakharov, B.A. (1976) X-Ray structure analysis of mixed-layer minerals, 256 p. Doklady Akademii nauk SSSR, Moscow.

Ferrage, E. (2004) Etude expérimentale de l'hydratation des smectites par modélisation des raies 00*l* de diffraction des rayons X—Implications pour l'étude d'une perturbation thermique sur la minéralogie de l'argilite du site Meuse-Haute Marne. Environnemental and Geochimistry Group, p. 326. Université Joseph Fourrier, Grenoble.

Ferrage, E., Lanson, B., Sakharov, B. A., and Drits, V. A. (2005) Investigation of smectite hydration properties by modeling of X-ray diffraction profiles. Part 1. Montmorillonite hydration properties. American Mineralogist, 90, 1358–1374.

Ferrage, E., Lanson, B., Sakharov, B. A., Jacquot, E., Geoffroy, N., and Drits, V. A. (2007a) Investigation of smectite hydration properties by modeling of X-ray diffraction profiles. Part 2. Influence of layer charge and charge location. American Mineralogist, 92, in press.

Ferrage, E., Kirk, C.A., Cressey, G., and Cuadros, J. (2007b) Dehydration of Ca-montmorillonite at the crystal scale. Part 1. Structure evolution. American Mineralogist, 92, 994–1006

Fogg, M., Price, S.J., Francis, R.J., O'Brien, S., and O'Hare, D (2000) Determination of the kinetics of crystallization of gibbsite using time resolved in situ energy dispersive powder diffraction. Journal of Materials Chemistry, 10, 2355–2357.

Friedman, H.L. (1964) Kinetics of thermal degradation of char-forming plastics from thermogravimetry. Application to phenolic plastic. Journal of Polymer Science Part C, Polymer Letters, 6, 183–195

Girgis, B.S. and Felix, N.S. (1987) Kinetic dehydroxylation of nontronite, estimated from isothermal and nonisothermal thermogravimetry. Journal of Thermal Analysis, 32, 1867–1876.

Girgis, B.S., El-Barawy, K.A., and Felix, N. S. (1987) Dehydration kinetics of some smectites: a thermogravimetric study. Thermochimica Acta, 111, 9–19.

Gualtieri, A.F. and Ferrari, S. (2006) Kinetics of illite dehydroxylation. Physics and Chemistry of Minerals, 33, 490–501.

Gualtieri, A.F., Belloto, M., Artioli, G., and Clark, S.M. (1995) Kinetic study of the kaolinite-mullite reaction sequence. Part II: Mullite formation. Physics and Chemistry of Minerals, 22, 215–222.

Guindy, N.M., El-Akkad, T.M., Flex, N.S., El-Massry, S.R., and Nashed, S. (1985) Thermal dehydration of mono- and di-valent montmorillonite cationic derivates. Thermochimica Acta, 88, 369–378.

Hancock, J.D. and Sharp, J.H. (1972) Method of comparing solid-state kinetic data and its application to the decomposition of kaolinite, brucite and $BaCO_3$. Journal of the American Ceramic Society, 55, 74–77.

Hulbert, S.F. (1969) Models for solid state reaction in powdered compacts: a review. Journal of the British Ceramic Society, 6, 11–20.

Laureiro, Y., Jerez, A., Rouquerol, F., and Rouquerol, J. (1996) Dehydration kinetics of Wyoming montmorillonite studied by controlled transformation rate thermal analysis. Thermochimica Acta, 278, 165–173.

Mazzucato, E., Artioli, G., and Gualtieri, A.F. (1999) High temperature dehydroxylation of muscovite-2M1: a kinetic study by in situ XRPD. Physics and Chemistry of Minerals, 26, 375–381.

Michot, L.J., Bihannic, I., Pelletier, M., Rinnert, E., and Robert, J.L. (2005) Hydration and swelling of synthetic Na-saponites: influence of layer charge. American Mineralogist, 90, 166–172.

Miletich, R., Zemann, J., and Nowak, M. (1997) Reversible hydration in synthetic mixite, $BiCu_6(OH)_6(AsO4)_3{\cdot}nH20$ ($n < 3$): hydration kinetics and crystal chemistry. Physics and Chemistry of Minerals, 24, 411–422.

Poinsignon, C., Yvon, J., and Mercier, R. (1982) Dehydration energy of the exchangeable cations in montmorillonite. A DTA study. Israel Journal of Chemistry, 22, 253–255.

Rausell-Colom, J.A., Fernandez, M., Serratosa, J.M., Alcover, J.F., and Gatineau, L. (1980) Organisation de l'espace interlamellaire dans les vermiculites monocouches et anhydres. Clay Minerals, 15, 37–58.

Redfern, S.A.T. (1987) The kinetics of dehydroxylation of kaolinite. Clay Minerals, 22, 447–456.

Rinnert, E., Carteret, C., Humbert, B., Fragneto-Cusani, G., Ramsay, J.D.F., Delville, A., Robert, J.L., Bihannic, I., Pelletier, M., and Michot, L.J. (2005) Hydration of a synthetic clay with tetrahedral charges: a multidisciplinary experimental and numerical study. Journal of Physical Chemistry B, 109, 23745–23759.

Sakharov, B.A. and Drits, V.A. (1973) Mixed-layer kaolinte-montmorillonite: a comparison observed and calculated diffraction patterns. Clays and Clay Minerals, 21, 15–17.

Sharp, J.H., Brindley, G.W., and Narahari Achar, B.N. (1966) Numerical data for some commonly used solid state reaction equations. Journal of the American Ceramic Society, 49, 379–382.

Simon, P. (2004) Isoconversional methods. Fudamentals, meaning and application. Journal of Thermal Analysis and Calorimetry, 76, 123–132.

Wilkinson, A.P., Speck, J.S., and Cheetham, A.K. (1994) In situ X-ray diffraction study of crystallization kinetics in $PbZr_{1-x}Ti_xO_3$ (PZT, $x = 0.0, 0.55, 1.0$). Chemistry of Materials, 6, 750–754.

Zabat, M. and Van Damme, H. (2000) Evaluation of the energy barrier for dehydration of homoionic (Li, Na, Cs, Mg, Ca, Ba, $Al_x(OH)_y^{z+}$ and La)-montmorillonite by a differentiation method. Clay Minerals, 35, 357–363.

Manuscript received July 25, 2006
Manuscript accepted March 2, 2007
Manuscript handled by Warren Huff